Deformable geometry model matching by topological and geometric signatures

Kwok-Leung TAM

Rynson W.H. LAW

Chong-wah NGO
Singapore Management University, cwngo@smu.edu.sg

Citation

Deformable Geometry Model Matching by Topological and Geometric Signatures

Kwok-Leung Tam [1]   Rynson W.H. Lau [1,2]   Chong-Wah Ngo [1]

[1] Department of Computer Science, City University of Hong Kong, Hong Kong
[2] Department of CEIT, City University of Hong Kong, Hong Kong

Abstract

In this paper, we present a novel method for efficient 3D model comparison. The method matches highly deformed models by comparing topological and geometric features. First, we propose "Bi-directional LSD analysis" to locate reliable topological points and rings. Second, based on these points and rings, a set of bounded regions are extracted as topological features. Third, for each bounded region, we capture additional spatial location, curvature and area distribution as geometric data. Fourth, to model the topological importance of each bounded region, we capture its effective area as weight. By using "Earth Mover Distance" as a distance measure between two models, our method can achieve a high accuracy in our retrieval experiment, with precision of 0.53 even at recall rate of 1.0.

1. Introduction

Due to the increasing popularity of 3D graphics and the high cost of geometry model creation, there is an increasing demand for model sharing. This motivates research on matching and retrieval of geometry models. Existing methods for model matching can be broadly grouped into three categories: geometric-based (GB), frequency-based (FB) and topological-based (TB). Unlike GB [5] and FB [8], TB is capable of handling deformable models, i.e., models representing the same object but in different postures. One representative approach in TB is MRG [1] which uses geodesic distance to construct a multi-resolution reeb graph for 3D objects. However, finding good approximation of geodesic distance among all pairs of vertices in a model is computationally expensive, which causes MRG to be slow in practice. In addition, because only area and length are considered in each node matching, probability of mismatching different models with similar skeleton can be high.

In this paper, we propose a model matching approach that integrates both topological and geometry cues for matching deformable models. To represent the skeleton of a model, we propose the "Bi-directional LSD Analysis" for topological points and rings extraction. To capture geometric information, the spatial location and surface distributions at topological rings are computed. The main contributions of this paper are:

- Our method analyzes a 3D model's skeletal representation by topological points and rings. This is relatively new among existing methods.

- With particular reference to MRG, our method tries to reduce the computation of geodesic by limiting the calculation at topologically important locations only. Since topological features are invariant to model tessellation, the number of geodesic calculations can be reduced to around one-third of [1] on average.

- Apart from skeletal matching, we also use additional geometry information to distinguish global surface of two models with similar skeleton. This area has not been explored in the previous topology methods.

- The proposed bi-directional LSD analysis, used for feature extraction here, can be further extended for skeleton extraction and model segmentation more efficiently and accurately on general geometry models.

The rest of the paper is organized as follows. Section 2 presents our Bi-directional LSD Analysis in detail. Sections 3 and 4 present our feature extraction method and our similarity measure, respectively. Section 5 presents and evaluates some experimental results. Finally, section 6 briefly concludes our work.

2. The Bi-directional LSD analysis

In [3], the "Level Set Diagram" (LSD) algorithm for constructing skeletons of geometry models based on critical points analysis is presented. There are three types of critical points: *minima*, *maxima* and *saddles*. For details of the method, we would refer readers to [3].

Though LSD is fast and can produce a tree structure to represent a 1D axial skeleton, it has two main problems. First, LSD performs poorly in identifying critical points when it is applied to general geometry models, which may have arbitrary curvature and probably noise. Second, the use of only one source point in LSD privileges a "slicing direction" [4], which may lead to missing of critical points. To extract topological points and rings reliably for our matching task, we proposed the Bi-directional LSD Analysis to address the two problems.

The Bi-directional LSD Analysis consists of two parts: *Modified LSD* and *Bi-directional Analysis*. The first part tries to improve LSD's performance on general models, while the second part tries to solve the "slicing direction" problem and prepares the features for model matching.

2.1 Modified LSD

We have observed that the major problem of LSD is its poor saddle identification on general models. To avoid such problem, we have developed a topological point

extraction method, which is a modified version of LSD, in our earlier publication. Due to page limitation, we would refer readers to [7] for the implementation details.

2.2 Bi-directional Analysis

After solving the noise problem, our Modified LSD still suffers from the "slicing direction" problem [4] because only one source point is used. To tackle this, we simply apply Modified LSD on the other furthest point to obtain the second LSD tree (bi-directional). Since the tree is obtained from another source point, the privileged "slicing direction" is now reversed and the missing vertices can now be found.

From our observation, Modified LSD works best on locating maximum and minimum critical points. In order to extract features reliably, we proposed to analyze a model from its maximum and minimum points first and Bi-directional Analysis is thus designed in a bottom-up manner. It consists of three steps: *clustering of local maximum vertices*, *protrusion region (PR) extraction*, and *segment region (SR) extraction*.

Notations: To simplify our discussion, we adopt the following notations for our analysis. Suppose we have a surface mesh $G = (V, E)$, where V is the set of vertices, E is the set of edges. Let $g_v(k, v)$, $g_{vs}(k, R)$ be the geodesic distance of k respect to a vertex v and vertex set R, respectively, and $path(k, v)$ be the shortest path, where $k, v \in V$ and $R \subset V$. Let also two furthest points [3] be $s_1, s_2 \in V$ and the two corresponding LSD skeletal trees be T_1 and T_2, such that $T_i = (V_i, E_i)$, where $V_i \subset V$ and $root(T_i) = s_i$ for $i=1,2$. We define $P(v)$ as the parent of vertex v within T_i, where $v \in V_i$. To further simplify our analysis, we consider two types of critical points only:

- Local Maximum M_i ={maxima and minima in V_i},
- Saddle Points S_i ={saddles in V_i}, $M_i \cup S_i = V_i, i=1,2$.

2.2.1 Clustering of Local Maximum Vertices

Since Modified LSD is best at locating local maximum, most of the vertices in M_1 and M_2 coincide and can be paired locally. We define a mv_cluster = $\{m, n\}$ where $n = f(m)$ and define *f(m)* as follows:

$$f(m) = \{n \mid g_v(n,m) \le g_v(P(m),m) \ and,$$
$$g_v(n,m) = Min_{k \in M_j}(g_v(k,m))\} \quad (1)$$

where $m \in M_i$, $P(m) \in S_i$, $n, k \in M_j$ and $i \ne j$

Normally, a mv_cluster contains two vertices m and $f(m)$. However, if $f(m) = \phi$, we simply let $n = m$, for our upcoming analysis.

2.2.2 Protrusion Region (PR) Extraction

After obtaining a series of mv_clusters, we can then extract Protrusion Region (PR) for our matching task. A

PR physically means the mesh region where protrusion tip resides. These regions include fingers, toes, ears, etc.

To define PR, we first find a *geodesic limit* (*l*) with respect to a starting seed z. Let $z, v_1, v_2, t \in V$ and $k \in \mathfrak{R}^3$, we define μ to be a segment ratio:

$$\mu = \frac{(\overrightarrow{t - v_1}) \bullet (\overrightarrow{v_2 - v_1})}{\left\| v_2 - v_1 \right\|^2} \quad (2)$$

such that $k = v_1 + \mu(v_2 - v_1)$ is the closest point to t. Assuming $g_v(v_1, z) \le g_v(v_2, z)$, *geodesic limit* is defined as:

$$l(t,z) = \begin{cases} g_v(v_1, z), & if \ \mu < 0 \\ (1 - \mu) \times g_v(v_1, z) + \mu \times g_v(v_2, z), & if \ 0 \le \mu \le 1 \\ g_v(v_2, z), & if \ \mu > 1 \end{cases} \quad (3)$$

Using the *geodesic limit*, we can define a new PR, PR_{new}, as the region bounded by a mv_cluster and its parent vertices *{{m, f(m)}, {P(m), P(f(m))}}*:

$$PR_{new} = \{t \mid g_v(t, x) \le l(t, x), \quad t \in \{V \setminus \cup PR_{old}\}\} \quad (4)$$

where $\cup PR_{old}$ are all the extracted PR so far and *geodesic limit l*, is defined by letting $v_1 = P(m)$, $v_2 = P(f(m))$, $z = \{x \mid Max_{x \in path(m, f(m))}(\|xv_1\| + \|xv_2\|)\}$, and x is a vertex on path$(m, f(m))$, which denoting the start vertex for the PR extraction. Let $neigh(t)$ be the one-ring neighborhood of t, boundary R_{PR} of the PR is then defined as:

$$R_{PR} = PR \setminus \{t \mid y = neigh(t), \quad t, y \in PR, \ \forall y \}, m, f(m) \in R_{PR} \quad (5)$$

2.2.3 Segment Region (SR) Extraction

After PR extraction, all the remaining regions are sequentially extracted as Segment Regions (SR). SR physically means the mesh region where significant branches occur, such as legs, arms and necks. By extending the idea of PR, we can extract SR similarly, where SR is defined exactly as PR except for two points:

1. SR is no longer originated from a start vertex x like PR. Instead, it is originated from the boundary of an existing PR or SR (R_{PR} or R_{SR}).
2. Since the starting seed is no longer a point x, but a boundary vertex set R, the geodesic distance function is also changed from $g_v(k, v)$ to $g_{vs}(k, R)$.

Hence, a new SR, SR_{new}, is defined as follows:

$$SR_{new} = \{t \mid g_{vs}(t, R) \le l(t, R), \ t \in \{V \setminus \{\cup PR + \cup SR_{old}\}\}\} \quad (6)$$

where $\cup PR + \cup SR_{old}$ are all the regions extracted so far and we define *geodesic limit l* by letting $v_1 = P'(m)$, $v_2 = P'(f(m))$, $z = R$, $m, f(m) \in R$ and $P'(m)$ defines the ancestor of m which is not yet visited by any PR or SR so far. The boundary of the SR, R_{SR}, is then defined as:

$$R_{SR} = SR \setminus \{t \mid y = neigh(t), \quad t \in SR, y \in \cup PR + \cup SR, \ \forall y\} \quad (7)$$

Eventually, a final mesh region will be left (e.g., the body of a human model). This last part is then extracted as a final SR, with boundary equals to the union of all the existing R adjacent to it.
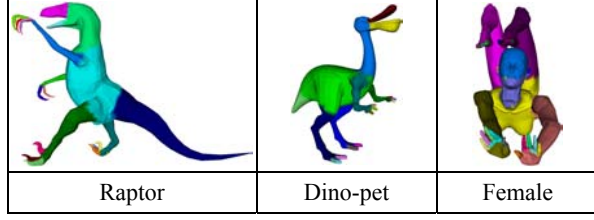
| Raptor | Dino-pet | Female |

Figure 2. Protrusion and segment regions.

Figure 2 shows the results after our extraction process. All PR and SR are colored differently. For the raptor and dino-pet models, nose, jaw, fingers, toes and tail are PR and neck, arms, legs and body are SR. For the female model, fingers, toes, ear tips, eye balls and mouth cavity are PR and arms, legs, neck, body are SR.

3. Feature Extraction

3.1 Topological Information

After Bi-directional LSD analysis, we obtain a set of local maximum clusters, together with a set of bounded regions $B = \cup PR + \cup SR$. Since the local maximum clusters are located at protrusion tips and the rings of boundary vertices (R) of both PR and SR are located at articulated joints, their existences actually represent the skeletal information of a model. Such features are invariant to model deformation. For the following sections, we consider the start vertex x in all PR as topological points and all vertex boundaries R as topological rings.

3.2 Geometric Information

To obtain geometric information for a model, we extract the following features to describe each bounded region $b \in B$.

3.2.1 Effective Area - Weights of Importance

As different bounded regions b have different importance, it is essential to capture such information in our features. We let effective area equals to the area of PR and SR.

3.2.2 Normalized Geodesic Sum - Spatial Information

To describe the spatial location of b, we use geodesic sum $G(t)$ as the spatial information. We compute $G(t)$ of a topological point as: $G(t) = \int_{p \in S} g_v(p,t) \partial S$. For a topological ring R, $G(R)$ is computed as:

$$G(R) = \frac{g_{vs}(o,R) \times G(w) + g_{vs}(w,R) \times G(o)}{g_{vs}(o,R) + g_{vs}(w,R)}$$

where $o = \{v \mid G(v) = Min_{q \in S}G(q)\}$ and w is the ancestor topological point of which R originates. Since all $b \in B$ are bounded by topological points and/or topological rings, geodesic sum $G(b)$ for B is calculated by averaging the surrounding $G(t)$ and/or $G(R)$. Finally, the normalized geodesic sum is then calculated as follows:

$$G_{norm}(b) = \frac{G(b) - Min_{q \in S}G(q)}{Max_{q \in S}G(q) - Min_{q \in S}G(q)}, \; b \in B \qquad (8)$$

In practice, $Max_{q \in S}G(q)$ actually equals to the maximum of all $G(t)$ calculated above. To find $Min_{q \in S}G(q)$ (i.e., vertex o), we have also developed a hierarchical approach which takes around 20 iterations to converge.

3.2.2 Surface Distribution – Geometric Surface data

To describe the global surface change with respect to $b \in B$, we use two feature vector K_1, K_2 (each of them is a 20-dimension histogram) to store the curvature and area information with respect to its topological ring as in Figure 3. After grouping all the vertices $v \in V$ with respect to geodesic distance $g_{vs}(v,R)$ into 20 intervals, we sum up all the curvature and area in the same interval to form the two feature vectors K_1, K_2.
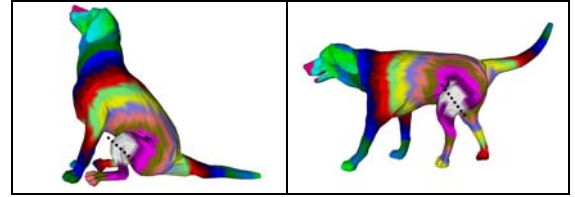

Figure 3. Vertices, v, of two surface meshes are partitioned into 20 bands with respect to $g_{vs}(v,R)$ from a topological ring R near the dogs' legs (the dash line).

4. Feature Matching

4.1 Distance Measure of Two Bounded Regions

To determine the similarity value of two bounded regions b_1, b_2, we use the following formula

$$Dist(b_1, b_2) = W_1 \times | G_{norm}(b_1) - G_{norm}(b_2) | \\ + W_2 \times L_{2,norm}(K_1(b_1), K_1(b_2)) + W_3 \times L_{2,norm}(K_2(b_1), K_2(b_2))$$

where W_1, W_2 and W_3 are ratios.

4.2 Distance Measure of Two Models

Since we have a set of bounded regions as model features and a distance measure between them, we can use Earth Mover Distance (EMD) [6] to compute the distance between two feature sets (signatures). Earth Mover Distance is a distance measure which calculates minimum amount of work that is required to transform one signature into another. By letting EMD weight equals to the effective area and letting the signature distance be $Dist( )$, we can compute the distance between two models.

5. Experimental Result

In our experimental database, there are 140 different models which are of different groups and postures. To test our method's invariant properties towards rotation and scaling, we prepare 3 additional sets by rotating against xy-axis, random scaling between (1.0, 2.0], and rotating by yz-axis plus random scaling to produce a total

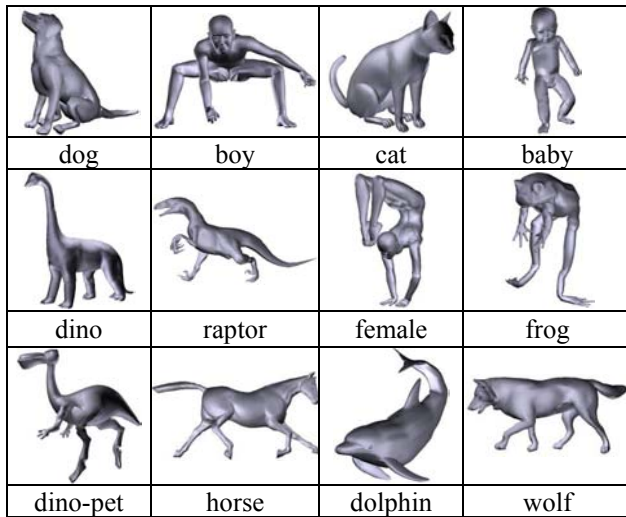of 560 models. We then manually categorize these models into 13 groups. 12 of them are shown in Figure 4.

dog	boy	cat	baby
dino	raptor	female	frog
dino-pet	horse	dolphin	wolf

Figure 4. 12 model groups in our model database.

Table 1. Mean Similarity of non-similar skeleton models.

	Boys	Frogs	Dolphins
Boys	1	0.214	0.033
Frogs	0.214	1	0.134
Dolphins	0.033	0.134	1

Table 2. Mean Similarity of similar skeleton models.

	Boys	Girls	Babies
Boys	1	0.850	0.684
Girls	0.850	1	0.599
Babies	0.684	0.599	1

Tables 1 and 2 show some of our matching results. We can see that our method can distinguish models based on their skeletons and shapes. For example in Table 1, boy, frog and dolphin are totally different models in term of skeletons. Their similarities are shown to have high contrast. In Table 2, boy, girl and baby models are similar models in term of skeleton, but different models in term of shapes. Our method can still distinguish them but with a smaller similarity difference. All these match human intuition correctly. Note that the similarity values are taken using all models and the value is normalized by maximum and minimum work done. Figure 5 shows the precision and recall graph of our method. It demonstrates that our method outperforms Geometry (D2) [5] and Frequency (Fourier) [8] which are shown to have good performance in [2].

6. Conclusions

This paper proposes a novel deformable geometry model matching method through analyzing models in both topological and geometric domains. Unlike existing topology methods [1], we use topological points and rings to represent skeletal information. As demonstrated in our experimental results, our method has a very high accuracy

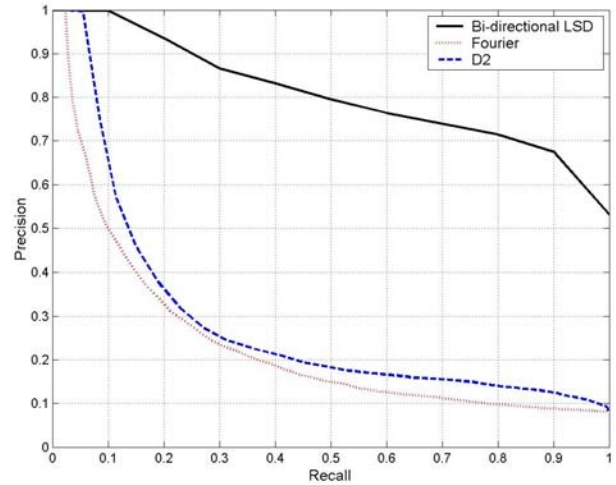in matching highly deformable models, invariant to rotation and scaling.

Figure 5. Precision and recall graph.

We have also presented our Bi-directional LSD analysis for capturing reliable topological points and rings in our application. Though it is currently used as a feature extraction tool, it can be further extended to drive skeleton extraction and model segmentation more efficiently and reliably on general 3D models.

Acknowledgements

References
[1] M. Hilaga, Y. Shinagawa, et al., "Topology Matching for Fully Automatic Similarity Estimation of 3D Shapes," *Proc. ACM SIGGRAPH*, pp. 203-212, Aug. 2001.

[2] R.W.H. Lau and B. Wong, "Web-Based 3D Geometry Model Retrieval," *World Wide Web Journal*, Kluwer Academic Publishers, 5(3):193-206, 2002.

[3] F. Lazarus and A. Verroust, "Level Set Diagrams of Polyhedral Objects," *Proc. ACM Symp. on Solid Modeling and Applications*, pp.130-140, 1999.

[4] M. Mortara, G. Patane, "Affine-Invariant Skeleton of 3D Shapes," *Proc. Shape Modeling International*, 2002

[5] R. Osada, T. Funkhouser, et al., "Matching 3D Models with Shape Distributions," *Proc. Shape Modeling*, May 2001.

[6] Y. Rubner, C. Tomasi, and L. Guibas, "A Metric for Distributions with Applications to Image Databases," *Proc. IEEE ICCV*, pp.59-66, 1998.

[7] K.L. Tam, R.W.H. Lau, and C.W. Ngo, "Deformable Geometry Model Matching Using Bipartite Graph," *Proc. Computer Graphics International*, June 2004.

[8] D. Vranic and D. Saupe, "3D Shape Descriptor based on 3D Fourier Transform," *Proc. EURASIP Conf. on DSP for Multimedia Communications & Services*, pp.271–274, 2001.